

Article

Polyphenylbenzene as a Platform for Deep-Blue OLEDs: Aggregation Enhanced Emission and High External Quantum Efficiency of 3.98%

Xuejun Zhan, Ning Sun, Zhongbin Wu, Jin Tu, Lei Yuan, Xi Tang, Yujun Xie, Qian Peng, Yong Qiang Dong, Qianqian Li, Dongge Ma, and Zhen Li

Chem. Mater., **Just Accepted Manuscript** • DOI: 10.1021/acs.chemmater.5b00094 • Publication Date (Web): 08 Feb 2015

Downloaded from <http://pubs.acs.org> on February 18, 2015

Just Accepted

“Just Accepted” manuscripts have been peer-reviewed and accepted for publication. They are posted online prior to technical editing, formatting for publication and author proofing. The American Chemical Society provides “Just Accepted” as a free service to the research community to expedite the dissemination of scientific material as soon as possible after acceptance. “Just Accepted” manuscripts appear in full in PDF format accompanied by an HTML abstract. “Just Accepted” manuscripts have been fully peer reviewed, but should not be considered the official version of record. They are accessible to all readers and citable by the Digital Object Identifier (DOI®). “Just Accepted” is an optional service offered to authors. Therefore, the “Just Accepted” Web site may not include all articles that will be published in the journal. After a manuscript is technically edited and formatted, it will be removed from the “Just Accepted” Web site and published as an ASAP article. Note that technical editing may introduce minor changes to the manuscript text and/or graphics which could affect content, and all legal disclaimers and ethical guidelines that apply to the journal pertain. ACS cannot be held responsible for errors or consequences arising from the use of information contained in these “Just Accepted” manuscripts.



Polyphenylbenzene as a Platform for Deep-Blue OLEDs: Aggregation Enhanced Emission and High External Quantum Efficiency of 3.98%

Xuejun Zhan,[†] Ning Sun,[‡] Zhongbin Wu,[‡] Jin Tu,[†] Lei Yuan,[†] Xi Tang,[§] Yujun Xie,[†] Qian Peng,^{||} Yongqiang Dong,[§] Qianqian Li,[†] Dongge Ma,^{*,‡} and Zhen Li^{*,†}

[†] Department of Chemistry, Hubei Key Lab on Organic and Polymeric Optoelectronic Materials, Wuhan University, Wuhan 430072, China

[‡] Changchun Institute of Applied Chemistry, the Chinese Academy of Sciences, Changchun 130022, China

[§] Department of Chemistry, Beijing Normal University, Beijing 100875, China

^{||} Institute of Chemistry, the Chinese Academy of Sciences, Beijing 100190, China

ABSTRACT: Great efforts have been devoted to seek novel approaches for the construction of efficient deep-blue fluorescent materials, one of the most important prerequisites for the commercialization of OLEDs. Here we report a new way to utilize polyphenylbenzene as a platform to yield a series of efficient deep-blue emitters. Non-doped multilayer electroluminescence (EL) devices using these new luminogens as emitting layers are fabricated. Maximum current efficiency (CE) of 2.0 cd A⁻¹ is achieved and the Commission Internationale de l'Éclairage (CIE) coordinates can stay at (0.15, 0.08), close to the saturated deep-blue (0.14, 0.08). Through rational design of the device structure, blue-violet emission with the CIE coordinates of (0.15, 0.06) can be realized. Furthermore, **10**-based doped devices show deep-blue emission with improved CE as high as 4.51 cd A⁻¹, and the external quantum efficiency (EQE) of 3.98%, which are among the best EL performance for deep-blue emission.

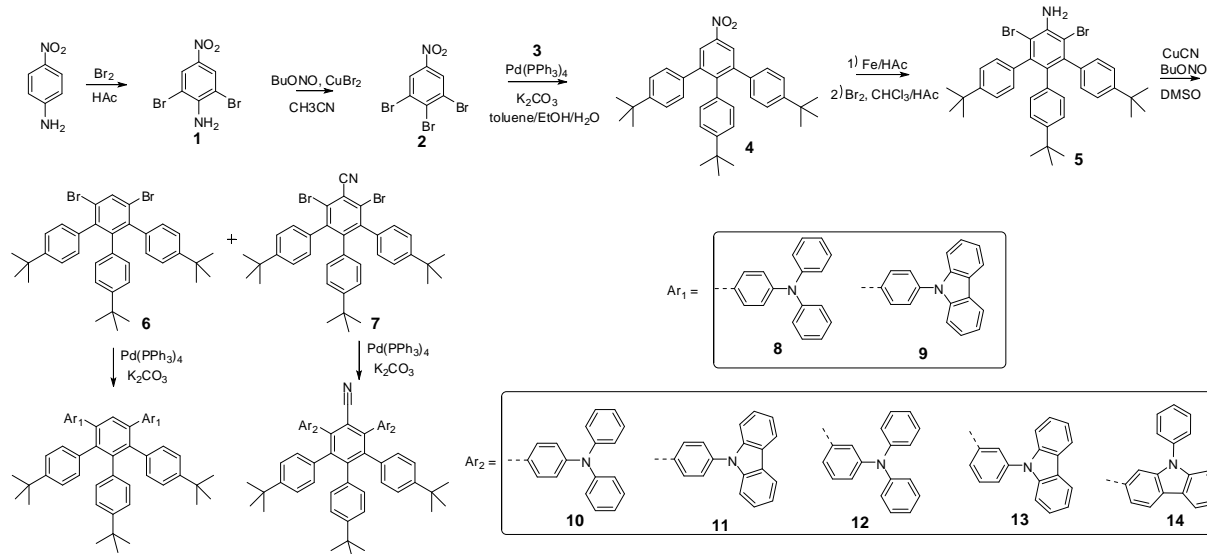
INTRODUCTION

Since the discovery of organic electroluminescence, through the unremitting efforts of scientists, Organic light-emitting devices (OLED) have been commercialized for applications in displays and solid state lightings.^{1,2} However, unlike their red and green counterparts with satisfactory performance, efficient and stable luminogens with standard blue or deep blue were still scarce, because of the intrinsic large bandgap and the encountered problems of stability.^{3,4} Through rational molecular design, many efficient emitters such as fluorene,⁵ anthracene,⁶ pyrene⁷ and carbazole⁸ derivatives with deep-blue emission have been synthesized. However, most of them give a light ranging within Commission Internationale de l'Éclairage (CIE) ($x < 0.15$, $y < 0.15$).^{9a} Actually, to further reduce the power consumption and generate light of other colors by energy cascade, it is badly needed to develop high efficient deep-blue emitters with CIE_y close to 0.08. Thanks to the great efforts of scientists, some deep-blue emitters have been obtained. For example, Lin *et al.* reported a deep-blue emitter of 3-[4-(1,1-dimesitylboryl)phenyl]-9-ethyl-9H-carbazole (CzPhB) at CIE (0.15, 0.09)

with a maximum EQE of 4.3%, and a relatively high turn-on-voltage (V_{on}) of 6.5 eV.^{9b} Chien *et al.* reported an emitter, 2-*tert*-butyl-9,10-bis[4'-(diphenylphosphoryl)phenyl]anthracene (POAn), with CIE coordinate of (0.15, 0.07) and the maximum CE up to 3.2 cd A⁻¹ (EQE of 4.5%),^{9c} while the degree of efficiency roll-off was obvious. Moorthy *et al.* even reported a pure deep-blue emitter with a CIE of (0.14, 0.08) from 3,3'-bis-*p*-(2,2-diphenylvinyl)-phenylbimesityl, with a moderate EQE of 1.51%.^{9d}

Another key point is the stability of the blue emission. Generally, most of the luminogens could exhibit excellent deep-blue or blue emission in solution, but in the solid state (the real state in LED devices), due to the molecular aggregation or π - π stacking, the emission would red-shift to longer wavelengths, leading to the blue-green light and lower efficiency, which was termed as "Aggregation Caused Quenching (ACQ) effect".¹⁰ Fortunately, through introducing bulk substituted groups or/and making the structure twisted, the problem of red-shifted emission could be inhibited, by sacrificing the efficiency or/and raising the turn-on-voltage,^{11,12} in most cases. Thus, if some blue or deep blue luminogens could be prepared conveniently with the characteristic of aggregation induc-

Scheme 1. Synthetic routes of the luminogens 8-14.



ed emission (AIE, a concept first proposed by Ben Zhong Tang in 2001) but not ACQ, the results should be excited.¹³ Actually, with tetraphenyl ethylene (TPE), a typical AIE luminogen with deep blue emission, as the basic building block, we have successfully obtained some good blue/deep blue AIE luminogens (which were recently named as AIEgens), by utilizing different linkage modes or/and increasing the twisting degree of the molecules in the presence of additional groups.¹⁴ However, the conjugation length of TPE is a little longer, leading to the difficulty to achieve good deep blue luminogens, and their lowest CIE_y value could only be 0.11, still higher than 0.08. Is it possible to further optimize the structure of this kind of promising AIEgens to design much better deep blue AIE luminogens? To realize this point, the conjugation length should be further shortened to some degree, while the AIE properties are remained.

Previously, we have designed a series of benzene-cored luminophores (Chart S1), which were AIE active and exhibited deep blue emission.¹⁵ Excitingly, even three carbazolyl groups were bonded to the benzene core, the maximum emission wavelength was as short as 401 nm, indicating its very short molecular conjugation length. Interestingly, once six phenyl groups were linked to a benzene core, the formed hexaphenylbenzene, studied intensively by Müllen *et al.*, is also a deep blue luminogen with the characteristic of aggregation enhanced emission (AEE), conquering the unwanted ACQ effect.¹⁶ However, so far, there were rarely reports concerning works using this star molecule as a platform to tune electron structure and apply them in OLEDs.^{17,18} The main reason might be the limitation caused by the traditional approach with the usage of alkyne and tetraphenylcyclopentadienone through the Diels-Alder reaction.¹⁹ To fully excavate the potential of hexaphenylbenzene for OLED applications, new methods of functionalization should be explored.

Inspired by all the points mentioned above, we designed a series of hexaphenylbenzene derivatives, **8-14**, mainly through step-by-step Suzuki coupling reaction. Carbazole and triphenylamine were introduced due to their good hole-transporting ability. Furthermore, we introduced cyano group to the center benzene so as to form donor- π -acceptor (D- π -A) type fluorophores, with the aim to make use of the effective radiative decay of their excited intramolecular charge-transfer (ICT) state.²⁰ For comparison, two molecules without cyano groups but hydrogen atoms were also synthesized. Nondoped devices based on **10** showed high performance with CE of 2.0 cd A⁻¹ and the CIE coordinates could stay at (0.15, 0.08), very close to the saturated deep-blue (0.14, 0.08). Excitedly, **10**-based doped devices exhibited deep-blue emission with more than doubled efficiency of 4.51 cd A⁻¹. Herein, we would like to present their syntheses, thermal, photo-physical, electrochemical and electroluminescent (EL) properties in detail.

RESULTS AND DISCUSSION

The seven new luminogens were obtained similarly through six synthetic steps with good yields (Scheme 1). Compound **4** was prepared through threefold Suzuki reaction between **2** and the commercial available **3** (4-*tert*-butylphenylboronic acid), then it was reduced by iron powder and followed by bromination reaction to yield **5**. The key intermediate **6** and **7** could be gotten in one step, when **5** was treated with CuCN and *t*-BuONO. Finally, through palladium (o)-catalyzed Suzuki cross-coupling reaction between **6/7** and 4-(diphenylamino)phenylboronic acid/4-(9H-carbazol-9-yl)phenylboronic acid/3-(diphenylamino)phenylboronic acid/3-(9H-carbazol-9-yl)phenylboronic acid/(9-phenyl-9H-carbazol-3-yl)boronic acid, compounds **8-14** could be synthesized with preferable yield. All these new compounds were

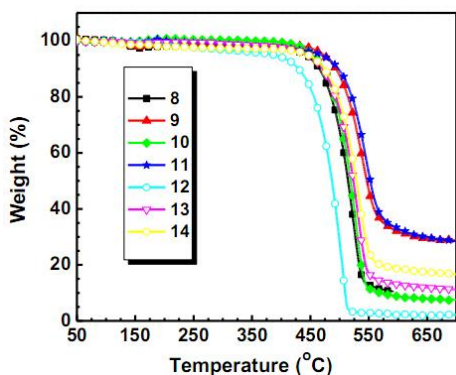


Figure 1. TGA curves of **8-14** recorded under N₂ at a heating rate of 10 °C/min.

purified by column chromatography on silica gel using petroleum ether-chloroform as eluent and fully characterized by ¹H and ¹³C NMR, mass spectrometry, and elemental analysis.

Generally, good thermal stability of the emitters is beneficial to the process of vacuum deposition and operating stability of OLED devices. The thermal properties of all these new compounds were investigated by thermogravimetric analysis (TGA) and differential scanning calorimetry (DSC) measurements. As depicted in Figure 1 and Table 1, all the luminogens are thermally stable with *T_d* (corresponding to 5% weight loss) values in the range of 390-473 °C. Owing to good thermal stability of carbazole, compounds contain carbazole units (**9**, **11**, **13**, and **14**) show better thermal stability than those bearing TPA units (**8**, **10**, and **12**). Generally, compounds with *para*-linkage mode show better thermal stability than the ones with *meta*-linkage way, owing to their more rigid conformations. Thus, among them, **9** and **11** (473 and 468 °C) possess higher decomposition temperatures than others. The glass transition temperatures (*T_g*) for **8**, **10**, **11**, **12**, **13** and **14** are 131, 128, 137, 101, 113 and 112 °C, respectively, further demonstrating their better thermal stability. Thus, the good thermal properties would benefit to the good performance of the corresponding LED devices.

All these compounds have good solubility in common organic solvents, such as dichloromethane, chloroform and tetrahydrofuran (THF) *et al.* Figure 2A and 3A show their absorption spectra in diluted THF solutions and thin solid films. In their solutions, compound **9**, **11**, **13**, **14** demonstrate similar absorptions, where the bands at about 330 and 290 nm should be ascribed to the intramolecular charge transfer (ICT) transition (Figure S2) and the carbazole-centered n-π* transition, respectively, while the bands around 340 nm are caused by the π-π* transition. **8**, **10**, **12** also exhibit similar absorptions, the bands around 300 nm could be attributed to the TPA-centered n-π* transition, and the shoulder band around 330 nm of **10** is mainly caused by the ICT transition. These absorption bands do not obviously red-shift in their thin solid films, since the periphery *tert*-butyl phenyl groups could

effectively suppress the possible intermolecular interactions.

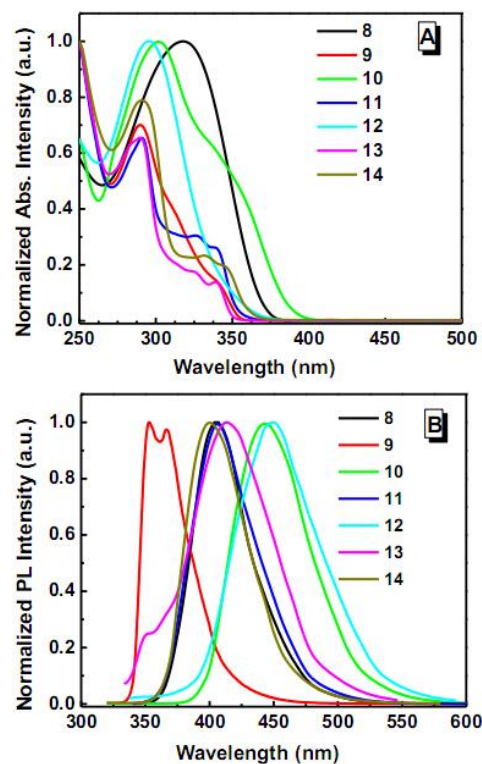


Figure 2. (A) UV spectra and (B) PL spectra of **8-14** in THF solution (~10 μM).

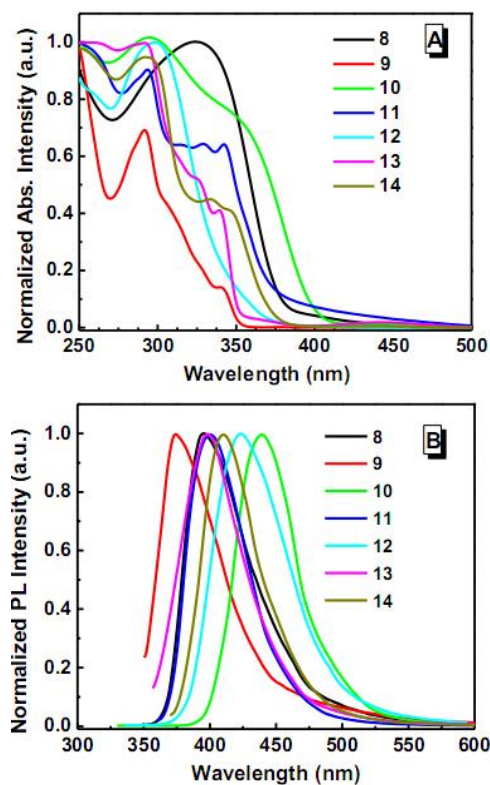


Figure 3. (A) UV and (B) PL spectra of **8-14** of the films.

Table 1. The thermal, electrochemical and photophysical data of the luminogens.

	T_d^a	T_g^b	E_g^c	E_{HOMO}^d	E_{LUMO}^e	PL λ_{em}		Φ_F (%)	$\lambda_{max,abs}$	
						solv ^f	film ^g		solv ^f	film ^g
	°C	°C	eV	eV	eV	nm	nm		nm	nm
TPA-TPA/ 8	442	131	3.33	-5.20	-1.87	406	396	58.7	316	323
Cz-Ph-Ph-Cz/ 9	473	---	3.50	-5.53	-2.03	367	374	34.3	341	342
TPA-CN-TPA/ 10	454	128	3.17	-5.26	-2.09	443	439	68.6	302(s330)	295(s338)
Cz-Ph-CN-Ph-Cz/ 11	468	137	3.48	-5.63	-2.15	406	401	80.3	340	342
mTPA-CN-mTPA/ 12	390	101	3.40	-5.26	-1.86	448	424	7.2	297	298
Cz-mPh-CN-mPh-Cz/ 13	445	113	3.54	-5.62	-2.08	412	394	6.4	340	339
Ph-Cz-CN-Cz-Ph/ 14	460	112	3.41	-5.60	-2.19	400	410	45.7	345	345

^a 5% weight loss temperature measured by TGA under N₂. ^b Glass-transition temperature measured by DSC under N₂. ^c Band gap estimated from optical absorption band edge of the solution. ^d Calculated from the onset oxidation potentials of the compounds. ^e Estimated using empirical equations $E_{LUMO} = E_{HOMO} + E_g$. ^f Determined in THF solution. ^g On glass. ^h Observed from absorption spectra in dilute THF solution, 10 μ M.

In the PL spectra, their emissions in diluted solutions mainly locate at 400-450 nm except compound **9** (367 nm). As a result of the intramolecular charge transfer derived from the introduced cyan group, the emissions of **10** (443 nm) and **11** (406 nm) red-shift 37 and 39 nm, in comparison with those of **8** (406 nm) and **9** (367 nm), respectively. In our previous study, the conjugation length of the whole molecules could be partially controlled by utilizing the different linkage mode of the different construction aromatic blocks. For example, just by changing the linkage mode of two TPE pieces from the *para* positions to *meta* ones, the maximum electroluminescent emission wavelengths of the resultant two BTPE derivatives in their LED devices could be adjusted from 488 nm to much blue-shifted one, 452 nm, as the result of the different conjugation effect between the two TPE moieties (Chart S2). However, when the linkage mode is changed from the *para* positions in **10** to *meta* ones in **12**, their maximum emission wavelengths are not with a big difference, but similar. Almost the same phenomenon is observed in the cases of **11** and **13**, disclosing the minor influence of the different linkage mode. This is reasonable. As demonstrated in Figure 5, all the luminogens are highly twisted, which directly lead to the weak conjugation effect between the constructing aromatic blocks. Thus, the different conjugation effects caused by the different linkage modes should be weakened by the highly twisted conformation, unlike those present in the cases of BTPE derivatives any longer.

In the PL spectra of their thin films, most of the luminogens exhibit narrow emissions with fwhm (full width at half-maximum) of about 50 nm. Compared to *para*-linkage **10** (439 nm), a slightly blue-shifted emission is found in the PL spectra of *meta*-linkage **12** (424 nm). Similar phenomenon could also be found in the cases of **11** and **13** (Table 1). As we aim to obtain blue/deep-blue OLEDs,

these blue shifted emissions are beneficial to achieve good performance. However, unlike most of the luminogens exhibit blue-shifted emissions in films compared to those in solution, **9** and **14** exhibit a little red shifted emission in solid state, indicating their relatively good coplanar conformation.

To quantitatively know the fluorescent properties of these luminogens, their absolute fluorescent quantum yields were measured (Table 1). The fluorescent quantum yields of **10** and **11** surpass 65%, owing to the suitably modified D- π -A molecular structures and their relatively good coplanarity, which could provide highly emissive ICT excited states upon excitation (Figure S2).^{20a} For **12** and **13**, due to their too highly twisted conformations, lower quantum yields were found.

In order to study the AEE characteristic of the seven luminogens, we chose cyclohexane and THF as the solvent pair for their miscibility, and recorded the photoluminescence (PL) change. Figure S3 show the PL spectra of the new fluorophores in THF/cyclohexane mixtures with different cyclohexane fractions (f_w), which enable fine-tuning of the solvent polarity and extent of solute aggregation. With gradual addition of cyclohexane, the PL intensities of all the seven compounds increase when cyclohexane content higher than 20%. Further increasing the cyclohexane content to 99%, in most cases, the emission intensities do not show decrease. Also, for comparison, the quantum yields of the luminogens were tested at different concentrations in THF solutions. From the absolute quantum yields in THF solutions and the mixtures of THF and cyclohexane (Figure S4), most of these luminogens demonstrate AEE characteristic.^{16b} Figure S4b show the absolute PLQYs of **8-14** in the THF/cyclohexane mixtures with different cyclohexane fractions (0, 20, 50, 80 and 99%). When the cyclohexane fraction was 20%, most of the PLQYs show some increase. This trend can even be maintained to 80% and 99% for compound **14** and **13**,

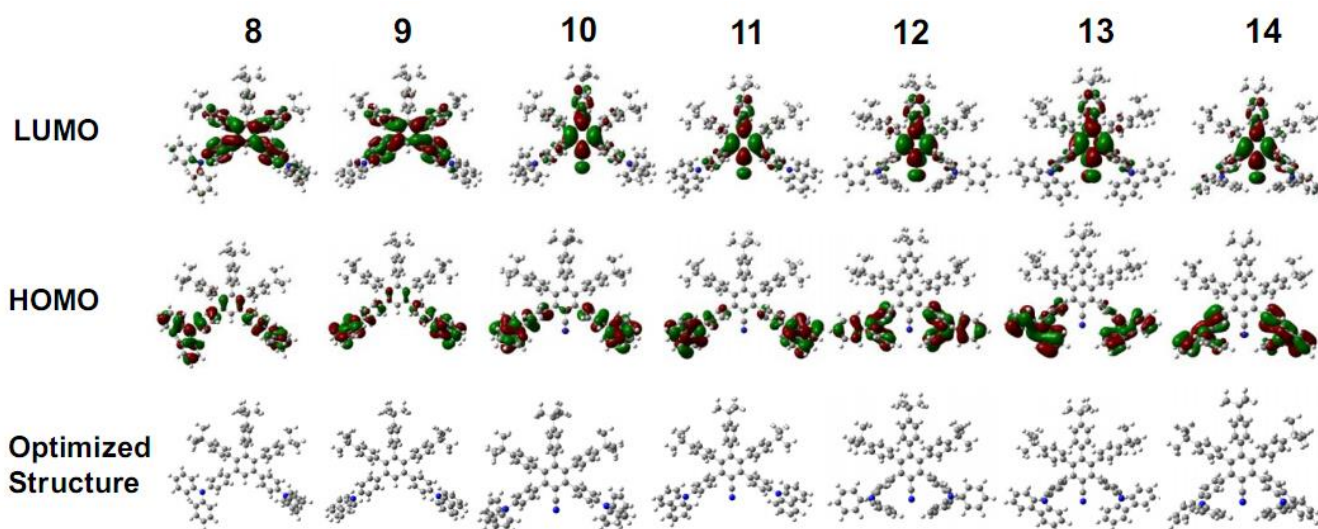


Figure 5. Calculated molecular orbital amplitude plots of HOMO and LUMO levels and optimized molecular structure.

respectively. Further increasing the cyclohexane fraction induced some decrease of PLQYs. This is not contradictory to our perspective of AEE and may be reasonable. At high concentration of cyclohexane, due to the poor solubility of the luminogens, the percentage of molecules inside the nanoparticles (which do not contribute to the PLQY) will increase.^{15,16b} Moreover, except **14**, the PL peaks show blue-shifted when the cyclohexane content is increased, probably due to the solvation effect (Figure S2) or/and the morphological change of the aggregates from amorphous to crystalline state. This is beneficial to the fabrication of deep blue light-emitting devices.

Thermally activated delayed fluorescence (TADF), developed by Adachi and co-workers, can lead to potentially 100% internal singlet yields through up-conversion of triplet to singlet states,^{2c} which opens up a new mind for electroluminescence. Considering that the highly twisted

structures are similar to some of Adachi's molecules (Chart S4), we also explored the potential TADF emission of our luminogens **10-14**. However, in their transient PL decay characteristics, all these luminogens exhibit first-order exponential decays, indicating no TADF emission present (Figure S5). Typically, the energy distance (ΔE_{ST}) between the lowest singlet state and the lowest triplet state should be small enough. To understand the absence of TADF emission, we tested the low-temperature fluorescence and phosphorescence (Figure S6). For **10**, **11**, **12**, **13** and **14**, their ΔE_{ST} values are calculated to be 0.43, 0.58, 0.41, 0.66 and 0.58 eV, respectively. As a result, in our case, these ΔE_{ST} values may not be small enough to guarantee the $T_1 \rightarrow S_1$ reverse intersystem crossing (ISC) process, while that of similar molecules in Adachi's work can be as small as 0.083 eV.^{2c}

Cyclic voltammetry (CV) measurements were carried out to investigate the electrochemical properties of these luminogens. The highest occupied molecular orbital (HOMO) energy levels were estimated from the onset oxidation potentials according to the equation: $HOMO = -(4.8 + E_{ox})$ eV, while the lowest unoccupied molecular orbital (LUMO) energy levels were obtained from optical band-gap energies (estimated from the onset wavelengths of the UV absorptions) and HOMO values. As shown in Figure 4 and Table 1, for **8**, **9**, **10**, **11**, **12**, **13** and **14**, their HOMO values are calculated to be -5.20, -5.53, -5.26, -5.63, -5.26, -5.62 and -5.60 eV, respectively. Some of them are a light higher than that of NPB (-5.30 eV), which could contribute to the device performance, due to the relatively easy transfer of holes. Their corresponding LUMO energy levels are calculated to be -1.87, -2.03, -2.09, -2.15, -1.86, -2.08 and -2.19 eV, respectively. The small energy gap between the emissive and hole-transporting layers suggests the efficient charge transfer in the OLEDs, thus low turn-

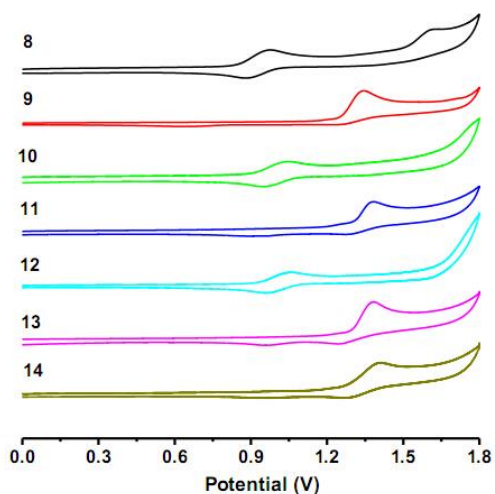


Figure 4. Cyclic voltammograms of compounds **8-14** recorded in dichloromethane.

Table 2. EL performances of **8** (A^a), **9** (B), **10** (C, H, I, J, K, L, M, N, O), **11** (D), **12** (E), **13** (F) and **14** (G).

device	λ_{EL} (nm)	V_{on}^b (V)	L_{max} (cd m ⁻²)	$\eta_{\text{P, max}}$ (lm w ⁻¹)	$\eta_{\text{C, max}}$ (cd A ⁻¹)	$\eta_{\text{ext, max}}$ (%)	CIE ^c (x, y)
A	420	3.5	734	0.35	0.44	0.72	0.16, 0.08
B	448	4.3	709	0.20	0.30	0.35	0.16, 0.08
C	445	3.3	2090	0.76	0.84	1.04	0.15, 0.07
D	450	3.5	1088	0.26	0.35	0.39	0.15, 0.08
E	451	3.7	922	0.27	0.34	0.33	0.15, 0.11
F	448	3.7	826	0.15	0.19	0.22	0.15, 0.09
G	449	3.7	1105	0.29	0.38	0.43	0.15, 0.09
H	431	3.3	3907	1.60	2.00	2.30	0.15, 0.08
I	441	3.3	1498	1.37	1.49	2.18	0.15, 0.06
J	424	4.5	3334	0.90	1.28	1.44	0.16, 0.10
K	427	4.1	4121	1.33	1.74	1.98	0.16, 0.09
L	430	3.7	5993	1.66	2.06	2.35	0.15, 0.09
M	431	3.6	4653	2.60	3.03	2.83	0.16, 0.11
N	432	3.6	5063	3.47	3.98	3.85	0.16, 0.11
O	428	3.4	4746	3.95	4.51	3.98	0.16, 0.11

^a Device configuration: ITO/MoO₃ (10 nm)/X/TPBi (30 nm)/LiF (1 nm)/Al; for device A-G: X = NPB(60 nm)/**8-14** (30 nm); for device H: X = NPB (60 nm)/mCP (10 nm)/**10** (30 nm); for device I: X = NPB (40 nm)/mCP (10 nm)/**10** (15 nm); for device J-O: X = NPB (60 nm)/mCP (10 nm)/BmPyPb: x% **10** (20 nm)/BmPyPb (10 nm), x = 5%(J), 10%(K), 20%(L), 30%(M), 40%(N), 50%(O). ^b Abbreviations: V_{on} = turn-on voltage at 1 cd m⁻², L_{max} = maximum luminance, $\eta_{\text{C, max}}$, $\eta_{\text{P, max}}$ and $\eta_{\text{ext, max}}$ = maximum power, current and external efficiencies, respectively. ^c CIE = Commission International de l'Éclairage coordinates at 6 V.

on voltages and high luminescence of the devices could be expected. Moreover, the large band-gaps of **12** (3.40 eV), **13** (3.54 eV), **14** (3.41 eV) demonstrate their relatively poor conjugation, owing to more twisted conformation by adopting *meta*-linkage mode or/and more crowd substitutions.

To further verify the structure-property relationship, we have carried out Density Functional Theory (DFT) calculations (B₃LYP/6-31g*) to obtain the optimized structures and orbital distributions of HOMO and LUMO energy levels of these luminogens. As demonstrated in Figure 5, the electron clouds of HOMO energy levels are all mainly located at the peripheral TPA or carbazole units, due to the good electron-donating abilities. For **10-14**, the LUMOs of the five luminogens are dominated by orbitals from the central cyano substituted benzene. And there is obvious separation of the HOMO and LUMO, which should benefit to the transfer of both holes and electrons. While for **8** and **9**, because of the week electron-withdrawing ability of benzene, the electron clouds of LUMO energy levels are more delocalized and HOMO-LUMO overlaps can be observed. In the optimized molecular structures of **8-14**, it is clearly seen that all the molecules adopt highly twisted structure and *meta*-linkage **12** and **13** are even more twisted than the *para*-linkage ones. Just because of the highly twisted conformations of these luminogens, the conjugation effect is largely decreased between the peripheral TPA and *tert*-butylphenyl moie-

ties and the phenyl core, directly leading to the designed deep blue emissions.

To investigate the EL performance of the new luminogens, seven nondoped fluorescent OLEDs were fabricated with a configuration of ITO/MoO₃ (10 nm)/NPB (60 nm)/X (30 nm)/TPBi (30 nm)/LiF (1 nm)/Al (Figure 6), in which MoO₃, NPB and TPBi worked as hole-injection, hole-transporting and hole-blocking layers, respectively. Performances of all these devices are shown in Table 2 (device A-G) and Figure S7. All the devices show deep-blue emission. Devices based on D- π -A type emitters turn on with the devices at lower voltage when compared with the devices based on **8** or **9**, indicating the smaller injection barriers between transporting layers and emitters. When the emitters adopt *meta*-linkage way (**12** and **13**) or connect carbazole unit at 3-position (**14**) so as to yield

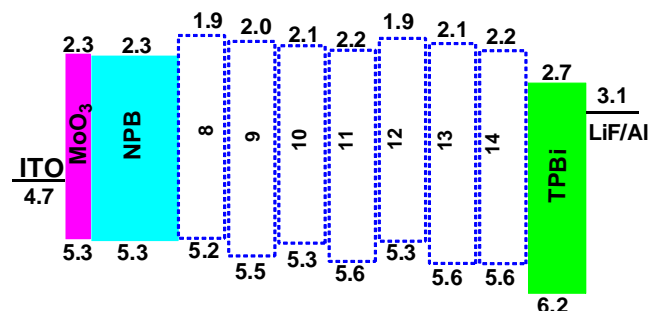


Figure 6. Energy level diagram of the nondoped devices.

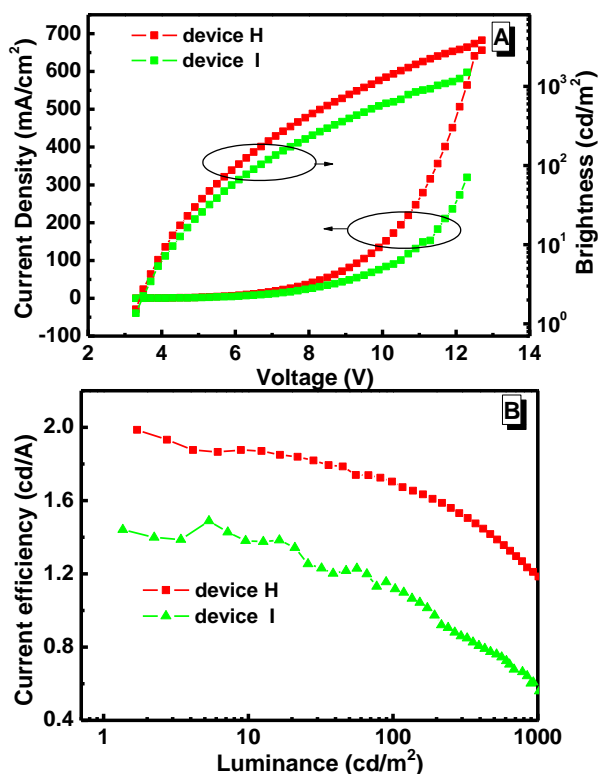


Figure 7. Change in current efficiency with the luminance in multilayer EL devices of **10**.

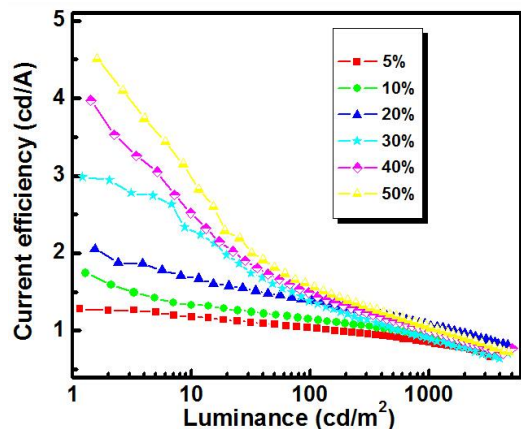


Figure 8. Change in current efficiency with the luminance in doped devices of **10** with different doping concentrations (5, 10, 20, 30, 40 and 50%).

highly twisted structure, V_{on} are raised, which are caused by bad conjugation. Among devices fabricated, the device based on compound **10** show the highest efficiencies with maximum EQE of 1.04%, CE of 0.84 cd A⁻¹, and PE of 0.76 lm W⁻¹. Meanwhile, the CIE coordinates of (0.15, 0.07), very close to the standard deep blue, was observed. And the EL spectra are almost identical at different driving voltages, indicating the stability of compound **10** as the emitting material layer (EML). Actually, the best performance of **10** may be reasonable. From the energy diagram (Figure 6), the HOMO levels of compound **8**, **10** and **12**

should be beneficial to the transfer of holes. Considering smaller gap between the emitter and EML can yield better injection of electrons.¹⁸ But the LUMO levels of **8** and **12** are a little bit higher (0.2 eV) than that of compound **10**. As a result, lower efficiencies were obtained. Compared to the devices based on **10**, lower EL efficiencies for **11** with maximum luminance (L_{max}) of 1088 cd m⁻² and maximum current efficiency ($\eta_{C, max}$) of 0.35 cd A⁻¹ may be ascribed to the different hole-transporting ability between carbazole and triphenylamine unit.

Next, we further optimized the device based on **10**. And additional layer of 1,3-di(9H-carbazol-9-yl)benzene (mCP) was added between NPB and EML with a configuration of ITO/MoO₃ (10 nm)/NPB (60 nm)/mCP (10 nm)/**10** (30 nm)/TPBi (30 nm)/LiF (1 nm)/Al in which mCP with wide band gap and high triplet state energy (E_T) functioned as the blocking layer to confine excitons in the EML.²¹ As shown in Figure 7 and Figure S8, compound **10** exhibit better efficiencies with CE of 2.0 cd A⁻¹, while the CIE_y could still remain 0.08.

Otherwise, it should be noted that the device I (Table 2) with a configuration of ITO/MoO₃ (10 nm)/NPB (40 nm)/mCP (10 nm)/**10** (15 nm)/TPBi (30 nm)/LiF (1 nm)/Al with compound **10** as EML can even exhibit blue-violet emission with the CIE coordinates of (0.15, 0.06) (Figure S8). And compared to device H, the decreased thickness of the layer of NPB and emitter do not show any influence on V_{on} . The maximum CE and EQE are 1.49 cd A⁻¹ and 2.18%, respectively. This result is among the best performance for nondoped OLEDs with CIE_y < 0.06 with the CIE_x remaining 0.15.^{18,20b} All these characteristics suggest that **10** is promising for the deep-blue OLED application.

From the low temperature phosphorescence characteristics, E_T value of **10** was estimated to be 2.63 eV. To further confine excitons in the EML and enhance the device performances of **10**-based devices, commercial available 1,3-bis(3,5-dipyrid-3-yl-phenyl)benzene (BmPyPb) (E_T = 2.70 eV) was selected to be the host for the fabrication of doped devices. Also, an additional layer of BmPyPb was inserted to enhance the transfer of electrons. Devices with the configuration of ITO/MoO₃ (10 nm)/NPB (60 nm)/mCP (10 nm)/BmPyPb: x% **10** (20 nm)/BmPyPb (10 nm)/TPBi (30 nm)/LiF (1 nm)/Al (Figure S13B) were constructed and tested (Figure 8, S11 and S12). The doped concentration is changed from 5 to 50%. At the doping concentration of 20%, the CIE coordinate of (0.15, 0.09) is obtained with good stability. The CIE_y suffers a modest increase when further increasing the doping concentration. Lower turn-on-voltages and better current efficiencies are observed when increasing the doping concentration. At a lower doping concentration of 5%, the current efficiency is 1.28 cd A⁻¹, then surpasses 2.0 cd A⁻¹ when the concentration is increased to 20%. When the concentration is further increased, the efficiency does not show some drop, disclosing the advantages of polyphenylbenzene and the designed twist

structure. Among the doped devices fabricated, device O employing 50% doped concentration as the EML could show deep-blue emission with maximum EQE of 3.98%, CE of 4.51 cd A⁻¹, and PE of 3.95 lm W⁻¹, which is among the best EL performance for deep-blue emission.^{18,20b} Generally, efficiency roll-off is significant for OLED devices. In these doped devices, similar to literature results,²² when the doping concentration is above 30%, the efficiencies show a relatively large degree of roll-off. For 100 mA cm⁻², the current efficiencies are decreased by 30, 32, 46, 65, 71 and 73%, for 5, 10, 20, 30, 40 and 50% doping concentration, respectively, showing that the roll-off is doping concentration dependent. This should be attributed to the singlet-singlet annihilation (SSA) and singlet-triplet annihilation (STA) processes,²³ or/and the carrier imbalance.^{22a}

CONCLUSIONS

In summary, through a new synthetic approach, by using polyphenylbenzene as a platform, novel deep-blue luminogens with D- π -A structure have been designed and synthesized. Due to the AEE properties of polyphenylbenzene, these luminogens exhibit enhanced emission. And most of the luminogens exhibit blue-shifted emissions in films compared to those in solution. All fabricated devices show deep-blue emission. Nondoped devices based on **10** display high performance with EQE, CE, and PE of 2.3%, 2.0 cd A⁻¹, and 1.6 lm W⁻¹, respectively, while the CIE coordinates can stay at (0.15, 0.08). Through rational design of the device structure, CIE coordinates of (0.15, 0.06) can be realized. Doped **10**-based devices demonstrate much improved performance with EQE and CE of 3.98% and 4.51 cd A⁻¹. Combined with CIE, all these characteristics suggest that **10** is a promising candidate for the deep-blue OLED application. Thus, the obtained experimental results might open up a new avenue to utilize polyphenylbenzene as a platform for the further development of efficient deep-blue luminogens.

ASSOCIATED CONTENT

Supporting Information

Experimental section, optimized structures, PL spectra in various solutions, low-temperature luminescence and phosphorescence and detailed devices performance. This material is available free of charge via the Internet at <http://pubs.acs.org/>.

AUTHOR INFORMATION

Corresponding Authors

* ("D. M."). E-mail: mdg1014@ciac.jl.cn.

* ("Z. L."). E-mail: lizhen@whu.edu.cn or lichemlab@163.com.

Notes

The authors declare no competing financial interest.

ACKNOWLEDGMENTS

We are grateful to the National Science Foundation of China (no. 21325416, 51333007), and the National Fundamental Key

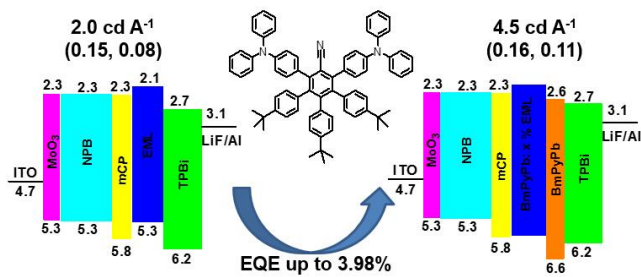
Research Program (2013CB834701, 2013CB834805) for financial support.

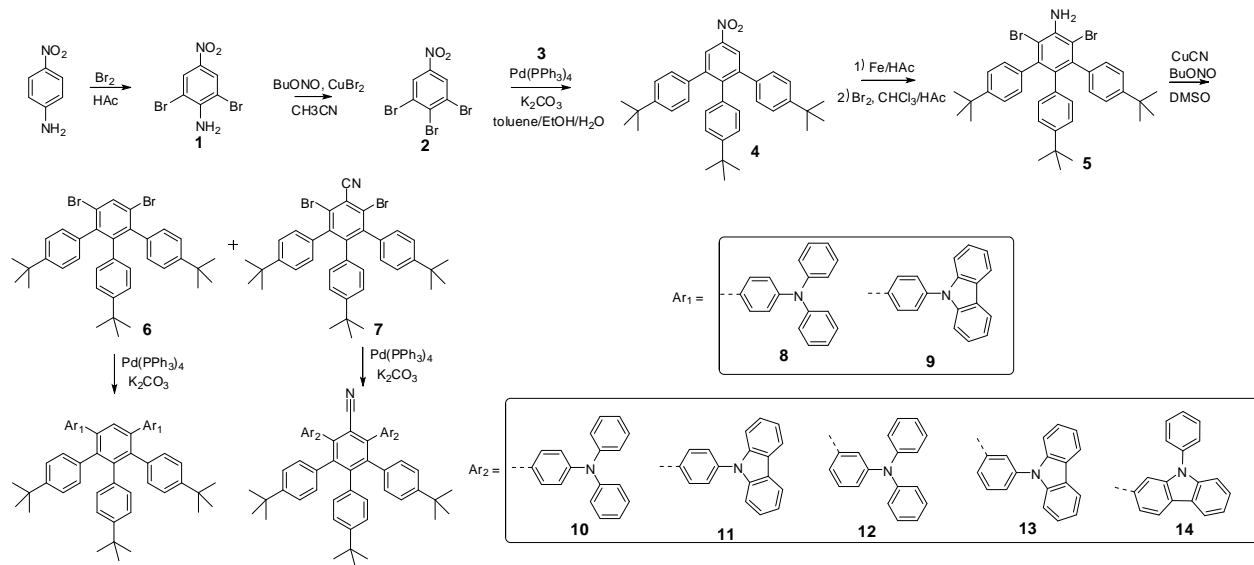
REFERENCES

- (1) Tang, C. W.; Vanslyke, S. A. *Appl. Phys. Lett.* **1987**, *51*, 913-917.
- (2) (a) Chao, T. C.; Lin, Y. T.; Yang, C. Y.; Hung, T. S.; Chou, H. C.; Wu, C. C.; Wong, K. T. *Adv. Mater.* **2005**, *17*, 992-996. (b) Li, H. Y.; Batsanov, A. S.; Moss, K. C.; Vaughan, H. L.; Dias, F. B.; Kamtekar, K. T.; Bryce, M. R.; Monkman, A. P. *Chem. Commun.* **2010**, *46*, 4812-4814. (c) Uoyama, H.; Goushi, K.; Shizu, K.; Nomura, H.; Adachi, C. *Nature* **2012**, *492*, 234-240.
- (3) (a) Farinola, G. M.; Ragni, R. *Chem. Soc. Rev.* **2011**, *40*, 3467-3482. (b) Gather, M. C.; Köhnen, A.; Meerholz, K. *Adv. Mater.* **2011**, *23*, 233-248.
- (4) (a) Kang, D. M.; Kang, J. W.; Park, J. W.; Jung, S. O.; Lee, S. H.; Park, H. D.; Kim, Y. H.; Shun, S. C.; Kim, J. J.; Kwon, S. K. *Adv. Mater.* **2008**, *20*, 2003-2007. (b) Park, T. J.; Jeon, W. S.; Park, J. J.; Kim, S. Y.; Lee, Y. K.; Jang, J.; Kwon, J. H.; Podo, R. *Appl. Phys. Lett.* **2008**, *92*, 113308-113308.
- (5) Polo, F.; Rizzo, F.; Gutierrez, M. V.; Cola, L. D.; Quici, S. J. *Am. Chem. Soc.* **2012**, *134*, 15402-15409.
- (6) (a) Kim, Y. H.; Jeong, H. C.; Kim, S. H.; Yang, K.; Kwon, S. K. *Adv. Funct. Mater.* **2005**, *15*, 1799-1805. (b) Zheng, C. J.; Zhao, W. M.; Wang, Z. Q.; Huang, D.; Ye, J.; Ou, X. M.; Zhang, X. H.; Lee, C. S.; Lee, S. T. *J. Mater. Chem.* **2010**, *20*, 1560-1566.
- (7) Zhao, Z. J.; Chen, S. M.; Lam, J. W. Y.; Lu, P.; Zhong, Y. C.; Wong, K. S.; Kwok, H. S.; Tang, B. Z. *Chem. Commun.* **2010**, *46*, 2221-2223.
- (8) Thomas, K. R. J.; Velusamy, M.; Lin, J. T.; Tao, Y. T.; Chuen, C. H. *Adv. Funct. Mater.* **2004**, *14*, 387-392.
- (9) (a) Xing, X.; Zhang, L. P.; Liu, R.; Li, S. Y.; Qu, B.; Chen, Z. J.; Sun, W. F.; Xiao, L. X.; Gong, Q. H. *ACS Appl. Mater. Interfaces.* **2012**, *4*, 2877-2880. (b) Lin, S. L.; Chan, L. H.; Lee, R. H.; Yen, M. Y.; Kuo, W. J.; Chen, C. T.; Jeng, R. J. *Adv. Mater.* **2008**, *20*, 3947-3952. (c) Chien, C. H.; Chen, C. K.; Hsu, F. M.; Shu, C. F.; Chou, P. T.; Lai, C. H. *Adv. Funct. Mater.* **2009**, *19*, 560-566. (d) Moorthy, J. N.; Venkatakrishnan, P.; Natarajan, P.; Lin, Z. H.; Chow, T. J. *J. Org. Chem.* **2010**, *75*, 2599-2609.
- (10) (a) Lemmer, U.; Heun, S.; Mahr, R. F.; Scherf, U.; Hopmeier, M.; Sieger, U.; Göbel, E. O.; Müllen, K.; Bäessler, H. *Chem. Phys. Lett.* **1995**, *240*, 373-378. (b) Jakubiak, R.; Collison, C. J.; Wan, W. C.; Rothberg, L. J. *J. Phys. Chem. A* **1999**, *103*, 2394-2398.
- (11) Lin, S. L.; Chan, L. H.; Lee, R. H.; Yen, M. Y.; Kuo, W. J.; Chen, C. T.; Jeng, R. J. *Adv. Mater.* **2008**, *20*, 3947-3952.
- (12) (a) Luo, J.; Zhou, Y.; Niu, Z. Q.; Zhou, Q. F.; Ma, Y. G.; Pei, J. *J. Am. Chem. Soc.* **2007**, *129*, 11314-11315. (b) Jiang, Z. Q.; Liu, Z. Y.; Yang, C. L.; Zhong, C.; Qin, J. G.; Yu, G.; Liu, Y. Q. *Adv. Funct. Mater.* **2009**, *19*, 3987-3995. (c) Yu, D. H.; Zhao, F. C.; Zhang, Z.; Han, C. M.; Xu, H.; Li, J.; Ma, D. G.; Yan, P. F. *Chem. Commun.* **2012**, *48*, 6157-6159.
- (13) (a) Luo, J. D.; Xie, Z. L.; Lam, J. W. Y.; Cheng, L.; Chen, H. Y.; Qiu, C. F.; Kwok, H. S.; Zhan, X. W.; Liu, Y. Q.; Zhu, D. B.; Tang, B. Z. *Chem. Commun.* **2001**, *37*, 1740-1741. (b) Wu, W. B.; Ye, S. H.; Huang, L. J.; Yu, G.; Liu, Y. Q.; Qin, J. G.; Li, Z. *Chin. J. Polym. Sci.* **2013**, *31*, 1432-1442. (c) Huang, J.; Chen, P. Y.; Yang, X.; Tang, R. L.; Wang, L.; Qin, J. G.; Li, Z. *Sci. China Chem.* **2013**, *56*, 1213-1220. (d) Huang, J.; Li, Q. Q.; Li, Z. *J. Mol. Eng. Mater.* **2013**, *1*, 1340006-1340008.
- (14) (a) Huang, J.; Sun, N.; Dong, Y. Q.; Tang, R. L.; Lu, P.; Cai, P.; Li, Q. Q.; Ma, D. G.; Qin, J. G.; Li, Z. *Adv. Funct. Mater.* **2013**, *23*, 2329-2337. (b) Huang, J.; Sun, N.; Chen, P. Y.; Tang, R. L.; Li, Q. Q.; Ma, D. G.; Li, Z. *Chem. Commun.* **2014**, *50*, 2136-2138.

- 1 (15) Zeng, Q.; Li, Z.; Dong, Y. Q.; Di, C. A.; Qin, A. J.; Hong, Y.
2 N.; Ji, L.; Zhu, Z. C.; Jim, C. K. W.; Yu, G.; Li, Q. Q.; Li, Z. A.; Liu,
3 Y. Q.; Qin, J. G.; Tang, B. Z. *Chem. Commun.* **2007**, *43*, 70-72.
4 (16) (a) Wang, C. G.; Wang, K.; Fu, Q.; Zhang, J. Y.; Ma, D. G.;
5 Wang, Y. J. *Mater. Chem. C* **2013**, *1*, 410-413. (b) Dong, S. C.; Li, Z.;
6 Qin, J. G. *J. Phys. Chem. B* **2009**, *113*, 434-441. (c) Hu, R. R.; Lam, J.
7 W. Y.; Liu, Y.; Zhang, X. A.; Tang, B. Z. *Chem. Eur. J.* **2013**, *19*,
8 5617-5624. (d) Bhalla, V.; Pramanik, S.; Kumar, M. *Chem. Com-*
9 *mun.* **2013**, *49*, 895-897. (e) Pramanik, S.; Bhalla, V.; Kumar, M.
10 *ACS Appl. Mater. Interfaces.* **2014**, *6*, 5930-5939.
11 (17) (a) Thomas, K. R. J.; Velusamy, M.; Lin, J. T.; Chuen, C. H.;
12 Tao, Y. T. *J. Mater. Chem.* **2005**, *15*, 4453-4459. (b) Xu, X. J.; Chen,
13 S. Y.; Yu, G.; Di, C. A.; You, H.; Ma, D. G.; Liu, Y. Q. *Adv. Mater.*
14 **2007**, *19*, 1281-1285. (c) Qin, T. S.; Zhou, G.; Scheiber, H.; Bauer, R.
15 E.; Baumgarten, M.; Anson, C. E.; List, E. J. W.; Müllen, K. *Angew.*
16 *Chem. Int. Ed.* **2008**, *47*, 8292-8296.
17 (18) Yuan, Y.; Chen, J. X.; Lu, F.; Tong, Q. X.; Yang, Q. D.; Mo, H.
18 W.; Ng, T. W.; Wong, F. L.; Guo, Z. Q.; Ye, J.; Chen, Z.; Zhang, X.
19 H.; Lee, C. S. *Chem. Mater.* **2013**, *25*, 4957-4965.
20 (19) Wu, J. S.; Pisula, W.; Müllen, K. *Chem. Rev.* **2007**, *107*, 718-
21 747.
22 (20) (a) Zhang, Q.; Li, J.; Shizu, K.; Huang, S. P.; Hirata, S.;
23 Miyazaki, H.; Adachi, C. *J. Am. Chem. Soc.* **2012**, *134*, 14706-14709.
24 (b) Ye, J.; Chen, Z.; Fung, M. K.; Zheng, C. J.; Ou, X. M.; Zhang, X.
25 H.; Yuan, Y.; Lee, C. S. *Chem. Mater.* **2013**, *25*, 2630-2637.
26 (21) (a) Méhes, G.; Nomura, H.; Zhang, Q. S.; Nakagawa, T.;
27 Adachi, C. *Angew. Chem. Int. Ed.* **2012**, *51*, 11311-11315. (b) Dias, F.
28 B.; Bourdakos, K. N.; Jankus, V.; Moss, K. C.; Kamekar, K. T.;
29 Bhalla, V.; Santos, J.; Bryce, M. R.; Monkman, A. P. *Adv. Mater.*
30 **2013**, *25*, 3707-3714. (c) Lee, S. Y.; Yasuda, T.; Yang, Y. S.; Zhang,
31 Q. S.; Adachi, C. *Angew. Chem. Int. Ed.* **2014**, *53*, 6402-6406.
32 (22) (a) Helander, M. G.; Morse, G. E.; Qiu, J.; Castrucci, J. S.;
33 Bender, T. P.; Lu, Z. *ACS Appl. Mater. Interfaces.* **2010**, *2*, 3147-
34 3152. (b) Im, Y.; Lee, J. Y. *Chem. Mater.* **2014**, *26*, 1413-1419.
35 (23) Murawski, C.; Leo, K.; Gather, M. *Adv. Mater.* **2013**, *25*,
36 6801-6827.
37
38
39
40
41
42
43
44
45
46
47
48
49
50
51
52
53
54
55
56
57
58
59
60

Table of Contents





Scheme 1. Synthetic routes of the luminogens 8-14.

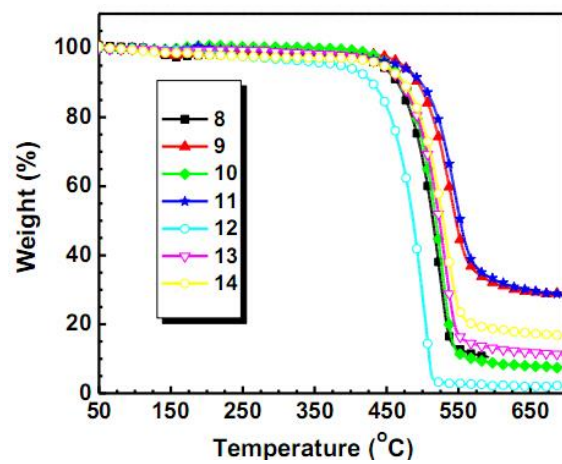


Figure 1. TGA curves of 8-14 recorded under N₂ at a heating rate of 10 °C/min.

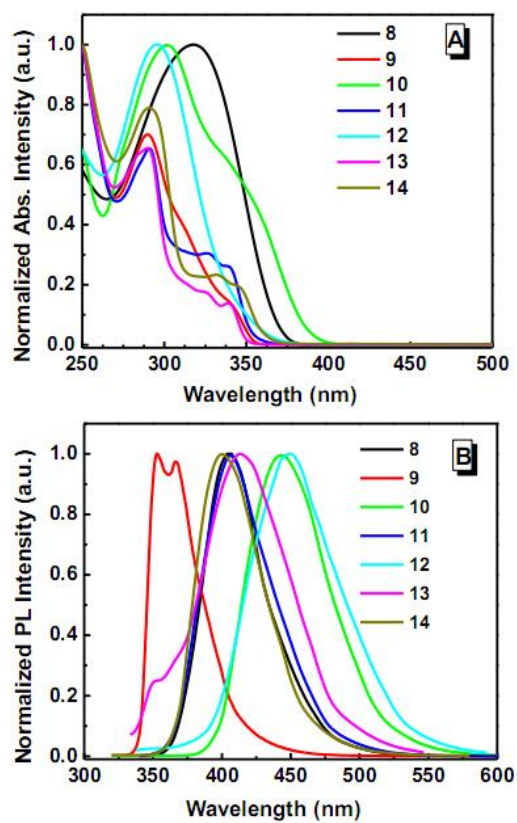


Figure 2. (A) UV spectra and (B) PL spectra of **8-14** in THF solution (~10 μM).

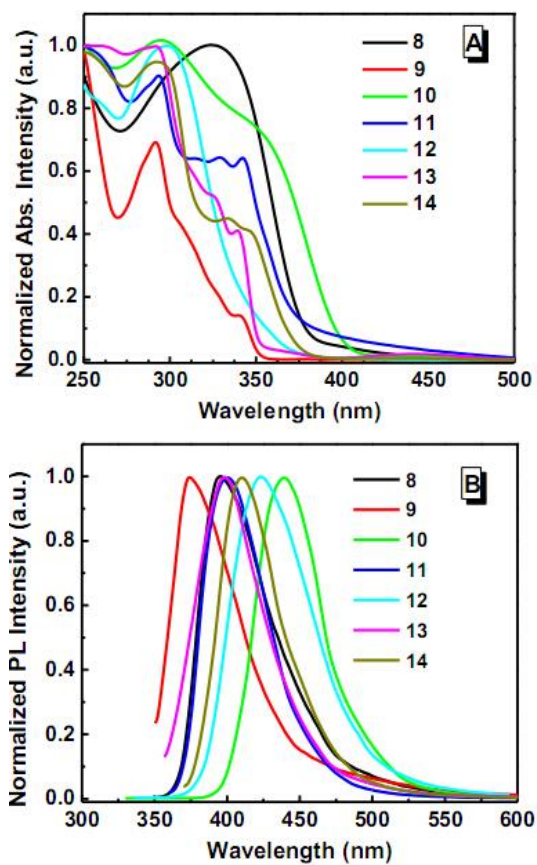


Figure 3. (A) UV spectra and (B) PL spectra of 8-14 of the films.

Table 1. The thermal, electrochemical and photophysical data of the luminogens.

	T_d^a	T_g^b	E_g^c	E_{HOMO}^d	E_{LUMO}^e	PL λ_{em}		Φ_F (%)	$\lambda_{max,abs}$	
						solv ^f	film ^g	solv ^f	solv ^h	film ^g
						nm	nm		nm	nm
TPA-TPA/ 8	442	131	3.33	-5.20	-1.87	406	396	58.7	316	323
Cz-Ph-Ph-Cz/ 9	473	---	3.50	-5.53	-2.03	367	374	34.3	341	342
TPA-CN-TPA/ 10	454	128	3.17	-5.26	-2.09	443	439	68.6	302(s330)	295(s338)
Cz-Ph-CN-Ph-Cz/ 11	468	137	3.48	-5.63	-2.15	406	401	80.3	340	342
mTPA-CN-mTPA/ 12	390	101	3.40	-5.26	-1.86	448	424	7.2	297	298
Cz-mPh-CN-mPh-Cz/ 13	445	113	3.54	-5.62	-2.08	412	394	6.4	340	339
Ph-Cz-CN-Cz-Ph/ 14	460	112	3.41	-5.60	-2.19	400	410	45.7	345	345

^a 5% weight loss temperature measured by TGA under N₂. ^b Glass-transition temperature measured by DSC under N₂. ^c Band gap estimated from optical absorption band edge of the solution. ^d Calculated from the onset oxidation potentials of the compounds. ^e Estimated using empirical equations $E_{LUMO} = E_{HOMO} + E_g$. ^f Determined in THF solution. ^g On glass. ^h Observed from absorption spectra in dilute THF solution, 10 μ M.

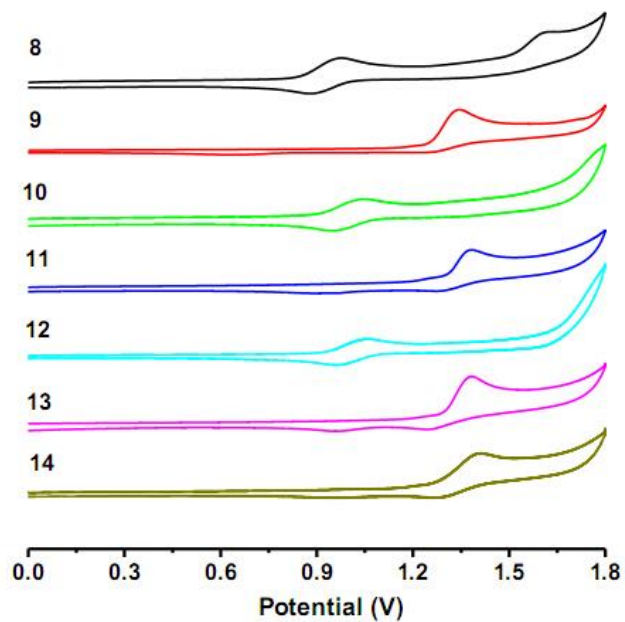


Figure 4. Cyclic voltammograms of compounds 8-14 recorded in dichloromethane.

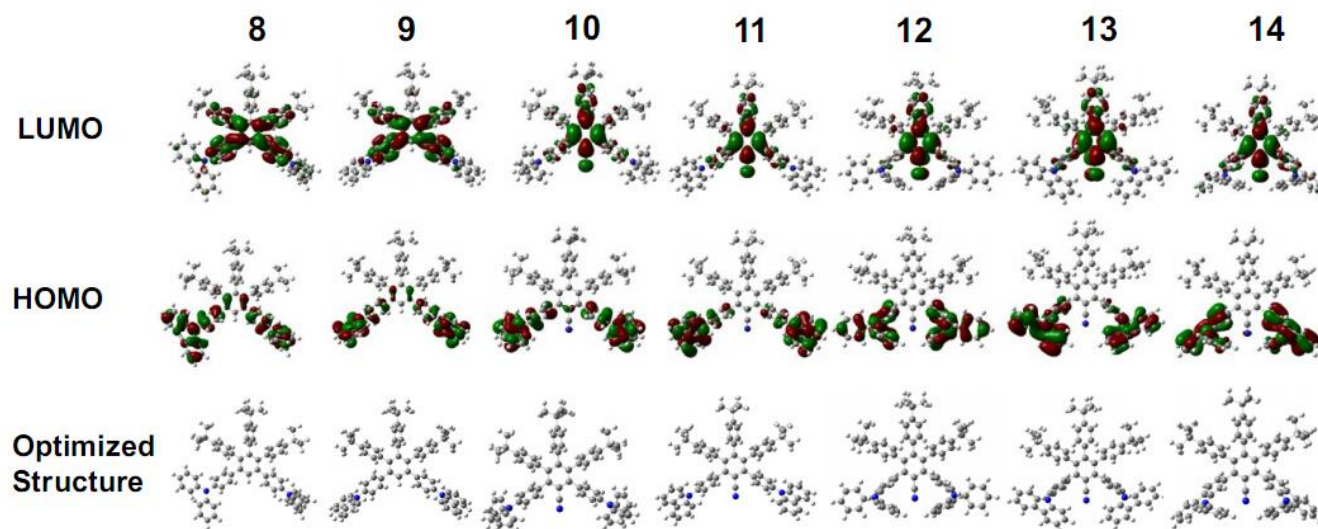


Figure 5. Calculated molecular orbital amplitude plots of HOMO and LUMO levels and optimized molecular structure.

Table 2. EL performances of **8** (A^a), **9** (B), **10** (C, H, I, J, K, L, M, N, O), **11** (D), **12** (E), **13** (F) and **14** (G).

device	λ_{EL} (nm)	V_{on}^b (V)	L_{max} (cd m ⁻²)	$\eta_{\text{P, max}}$ (lm w ⁻¹)	$\eta_{\text{C, max}}$ (cd A ⁻¹)	$\eta_{\text{ext, max}}$ (%)	CIE ^c (x,y)
A	420	3.5	734	0.35	0.44	0.72	0.16, 0.08
B	448	4.3	709	0.20	0.30	0.35	0.16, 0.08
C	445	3.3	2090	0.76	0.84	1.04	0.15, 0.07
D	450	3.5	1088	0.26	0.35	0.39	0.15, 0.08
E	451	3.7	922	0.27	0.34	0.33	0.15, 0.11
F	448	3.7	826	0.15	0.19	0.22	0.15, 0.09
G	449	3.7	1105	0.29	0.38	0.43	0.15, 0.09
H	431	3.3	3907	1.60	2.00	2.30	0.15, 0.08
I	441	3.3	1498	1.37	1.49	2.18	0.15, 0.06
J	424	4.5	3334	0.90	1.28	1.44	0.16, 0.10
K	427	4.1	4121	1.33	1.74	1.98	0.16, 0.09
L	430	3.7	5993	1.66	2.06	2.35	0.15, 0.09
M	431	3.6	4653	2.60	3.03	2.83	0.16, 0.11
N	432	3.6	5063	3.47	3.98	3.85	0.16, 0.11
O	428	3.4	4746	3.95	4.51	3.98	0.16, 0.11

^a Device configuration: ITO/MoO₃ (10 nm)/X/TPBi (30 nm)/LiF (1 nm)/Al; for device A-G: X = NPB(60 nm)/**8-14** (30 nm); for device H: X = NPB (60 nm)/mCP (10 nm)/**10** (30 nm); for device I: X = NPB (40 nm)/mCP (10 nm)/**10** (15 nm); for device J-O: X = NPB (60 nm)/mCP (10 nm)/BmPyPb: x% **10** (20 nm)/BmPyPb (10 nm), x = 5%(J), 10%(K), 20%(L), 30%(M), 40%(N), 50%(O). ^b Abbreviations: V_{on} = turn-on voltage at 1 cd m⁻², L_{max} = maximum luminance, $\eta_{\text{P, max}}$, $\eta_{\text{C, max}}$ and $\eta_{\text{ext, max}}$ = maximum power, current and external efficiencies, respectively. ^c CIE = Commission International de l'Éclairage coordinates at 6 V.

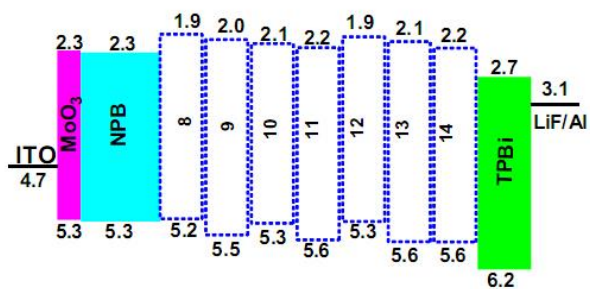


Figure 6. Energy level diagram of the nondoped devices.

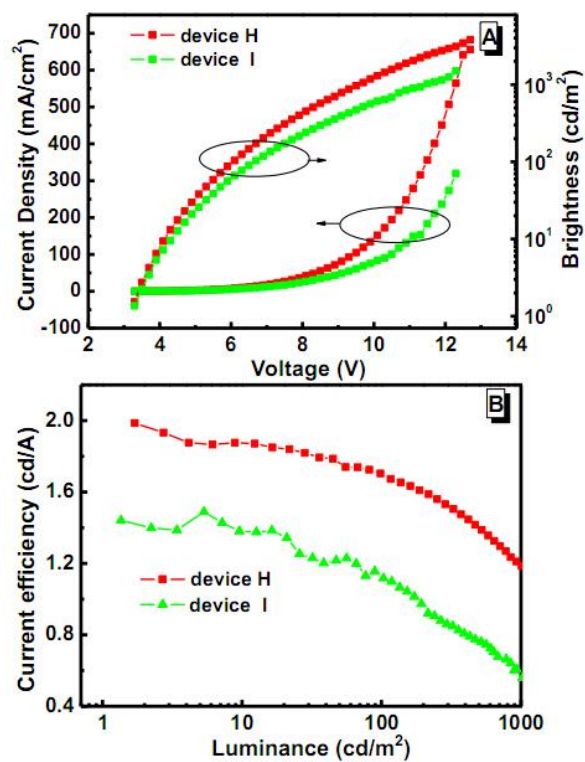


Figure 7. Change in current efficiency with the luminance in multilayer EL devices of 10.

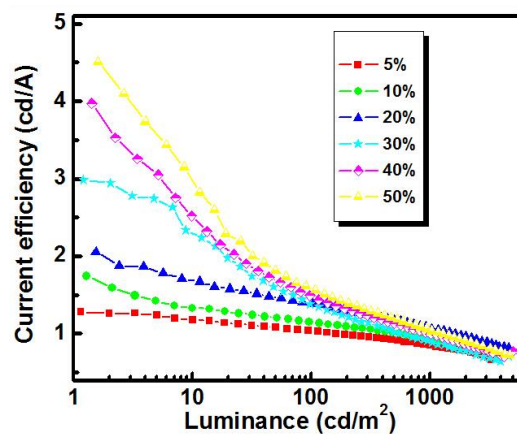


Figure 8. Change in current efficiency with the luminance in doped devices of **10** with different doping concentrations (5%, 10%, 20%, 30%, 40% and 50%).